Influence of Pulmonary Surfactant Protein B on Model Lung Surfactant Monolayers

ARTICLE *in* LANGMUIR · MARCH 2002

Impact Factor: 4.46 · DOI: 10.1021/la015702w · Source: OAI

Influence of Pulmonary Surfactant Protein B on Model Lung Surfactant Monolayers

Frank Bringezu,*,† Junqi Ding, Gerald Brezesinski,‡ Alan J. Waring,§ and Joseph A. Zasadzinski

Department of Chemical Engineering, University of California, Santa Barbara, California 93106-5080

Received November 28, 2001

Pressure−area isotherms, Brewster angle microscopy, and grazing incidence X-ray diffraction measurements reveal that human lung surfactant protein SP-B_{1-78} and the dimer of the amino terminus dSP-B_{1-25} modify the phase behavior of lipid mixtures consisting of dipalmitoylphosphatidylcholine/palmitoyl-oleyl-phosphatidylglycerol/palmitic acid (DPPC/POPG/PA). The addition of SP-B increases the fraction of fluid phase in the liquid-expanded/liquid-condensed two-phase region. Brewster angle microscopy enabled the visualization of a fluid network, which separates the condensed phase domains. This network is stabilized by SP-B adsorption. GIXD measurements show that SP-B also alters the structure of the condensed chain lattice leading to higher tilt and increased area per hydrocarbon chain. The comparison of SP-B_{1-78} with the shorter peptide dSP-B_{1-25} exhibits, that the dimer alters the lipid order more drastically. The larger effects found for dSP-B_{1-25} were explained using a model that assumes a partial incorporation of the peptide into the layer. The specific behavior of the dimer could enhance the activity of the peptide as found in recent animal model studies. This is the first investigation showing a systematic influence of SP-B on the condensed chain lattice of phospholipids, thus verifying that SP-B not only interacts with the expanded phase, but also interactions with the condensed phase lipids have to be taken into account which might be essential for proper peptide function.

Introduction

Lung surfactant is a complex mixture of lipids and specific proteins that is expressed by the alveolar type II cells in order to form a monolayer at the liquid−air interface in the lung alveoli. Proper lung function requires low surface tension provided by lung surfactants in order to minimize the work of breathing.[1−3] Although native surfactant is a multicomponent, lipid−protein mixture,[3−5] key components have been identified that provide simplified model mixtures mimicking many of the features of native lung surfactants both in vitro and in vivo.[4−11] These are saturated dipalmitoylphosphatidylcholine (DPPC), unsaturated phophatidylglycerols (PG) and palmitic acid (PA) as the main lipid components[8,12,13] and the lung surfactant-specific apoproteins B and C.[14]

The multiple lipid and protein components are necessary because of the conflicting requirements of the surfactant monolayer. Rigid monolayers formed by DPPC alone can provide the necessary low surface tension on compression of the alveolar interface that accompanies exhalation. However, during the expansion that occurs on inhalation, the rapid spreading or adsorption of pure DPPC to cover the new interface is not possible.[15,16] On the other hand, fluid, fast-spreading unsaturated PG's cannot sufficiently lower the surface tension.[11]

Surfactant protein B (SP-B) is a small (amino acid residues 1−79; $M_r \sim 8700$), lipid-associating protein, which is found in mammalian lung surfactant as a disulfide-linked homodimer.[17] SP-B belongs to the saposin family of proteins, and exhibits charge-dependent, amphipathic alpha-helical structure in membrane-like environments. This surfactant protein has been shown to play critical roles in lung function, since its deficiency caused by mutations in the SP-B gene results in lethal respiratory distress in either humans[18] or knock-out mice.[19] Using a mouse model system, Beck et al. (2000) recently demonstrated[20] that optimal activities of SP-B in vivo and in

* Corresponding author. Institute of Biophysics and X-ray Research, Schmiedlstrasse 6, A-8042 Graz, Austria. Phone: +43-316-4120-332. FAX: +43-316-4120-390. E-mail: bringezu@denet.de..

† Current working address: Inst. of Biophysics and X-ray research, Schmiedlstrasse 6, A-8042 Graz, Austria.

‡ Max Planck Institute of Colloids and Interfaces, Am Muehlenberg 1, D-14476 Golm/Potsdam, Germany.

§ Department of Medicine, UCLA and Department of Pediatrics, Harbor-UCLA, Los Angeles, CA 90095.

(1) Schürch, S.; Goerke, J.; Clements, J. A. *Proc. Nat. Acad. Sci. U.S.A.* **1976**, *73*, 4698−4702.

(2) Schürch, S.; Goerke, J.; Clements, J. A. *Proc. Nat. Acad. Sci. U.S.A.* **1978**, *75*, 3417−3421.

(3) Goerke, J. *Biochim. Biophys. Acta* **1998**, *1408*, 79−89.

(4) Mizuno, K.; Ikegami, M.; Chen, C. M.; Ueda, T.; Jobe, A. H. *Pediatr. Res.* **1995**, *37*, 271−276.

(5) Pison, U.; Herold, R.; Schürch, S. *Colloids Surf.* **1996**, *114*, 165−184.

(6) Tanaka, Y.; Takei, T.; Aiba, T.; Masuda, K.; Kiuchi, A.; Fujiwara, T. *J. Lipid Res.* **1986**, *27*, 475−485.

(7) Cochrane, C. G.; Revak, S. D. *Science* **1991**, *254*, 566−568.

(8) Johansson, J.; Gustafsson, M.; Zaltash, S.; Robertson, B.; Curstedt, T. *Biol. Neonate* **1998**, *74*, 9−14.

(9) Lipp, M. M.; Lee, K. Y. C.; Takamoto, D. Y.; Zasadzinski, J. A.; Waring, A. J. *Phys. Rev. Lett. (USA)* **1998**, *81*, 1650−1653.

(10) Bernhard, W.; Mottaghian, J.; Gebert, A.; Rau, G. A.; von der Hardt, H.; Poets, C. F. *Am. J. Crit. Care Med.* **2000**, *162*, 1524−1533.

(11) Ding, J.; Takamoto, D. Y.; Lipp, M. M.; von Nahmen, A.; Lee, K. Y. C.; Waring, A. J.; Zasadzinski, J. A. *Biophys. J.* **2001**, *2001*, 2262−2272.

(12) Hawgood, S.; Derrick, M.; Poulain, F. *Biochim. Biophys. Acta* **1998**, *1408*, 150−160.

(13) Veldhuizen, R.; Nag, K.; Orgeig, S.; Possmayer, F. *Biochim. Biophys. Acta* **1998**, *1408*, 90−108.

(14) Johansson, J.; Curstedt, T.; Robertson, B. *Eur. Respir. J.* **1994**, *7*, 372−391.

(15) Poulain, F. R.; Clements, J. A. *West. J. Med.* **1995**, *162*, 43−50.

(16) Robertson, B.; Halliday, H. L. *Biochim. Biophys. Acta* **1998**, *1408*, 346−361.

(17) Patthy, L. *J. Biol. Chem.* **1991**, *266*, 6034−6037.

(18) Nogee, L. M.; Garnier, G.; Dietz, H. C.; Singer, L.; Murphy, A. M.; deMello, D. E.; Colten, H. R. *J. Clin. Invest.* **1997**, *93*, 1860−1863.

(19) Tokieda, K.; Whitsett, J. A.; Clark, C.; Weaver, T. E.; Ikeda, K.; McConnell, K. B.; Jobe, A.; Ikegami, M.; Iwamoto, H. S. *Am. J. Physiol.* **1997**, *273*, L875-L882.

10.1021/la015702w CCC: $22.00
Published on Web 01/31/2002

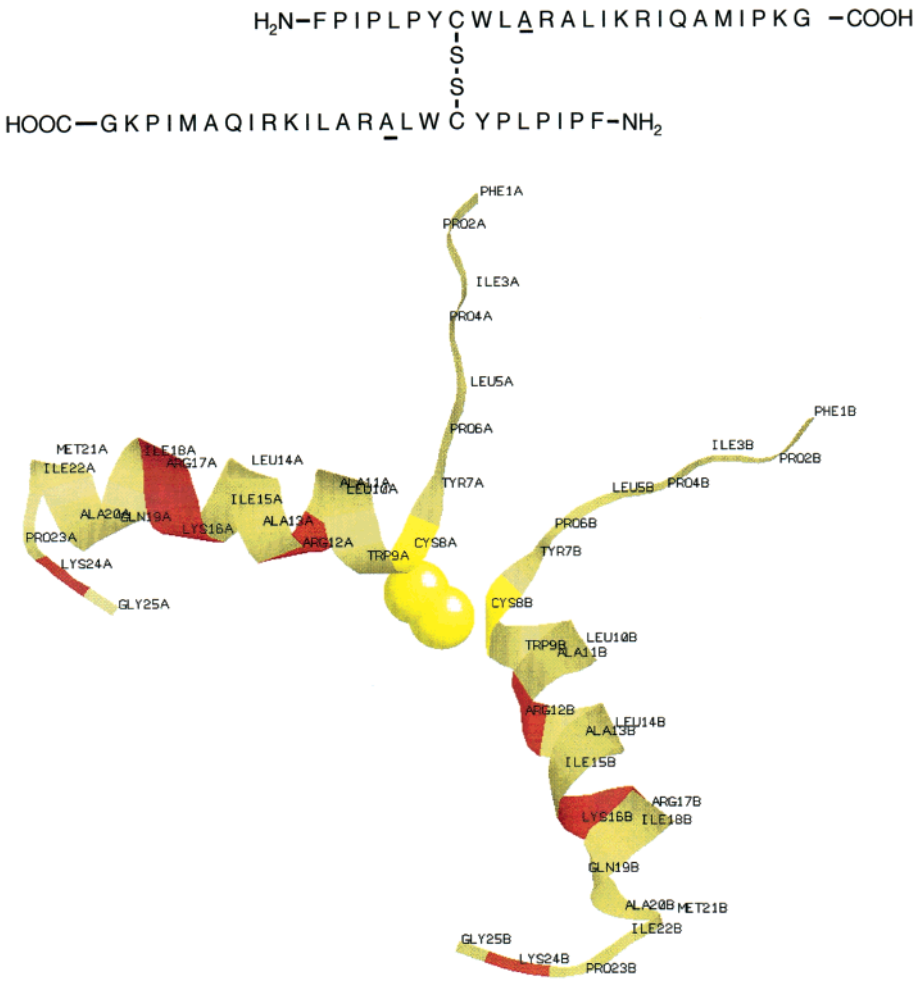

Figure 1. Ribbon diagram of the N-terminal sequence of dSP-B_{1-25} (data constructed from the monomer coordinates in PDB: 1DFW) of the full length human SP-B_{1-79}. The polar regions of the sequence are colored red. The amino acid sequence is given on top and the labels are shown in the ribbon diagram.

vitro were associated with the homodimeric form of the molecule. Interestingly, construction of a disulfide-linked, homodimer SP-B peptide, which includes both the N-terminal insertion sequence (residues 1−8) and the adjacent N-terminal amphipathic helix (residues 9−25), produced a synthetic mimic peptide (i.e., dSP-B_{1-25}, see Figure 1) that emulates many of the enhanced surface activities of the native, full-length dimeric SP-B protein.[21] Moreover, the benefit of the dimer over the full length SP-B monomer was suggested; however, the molecular mechanism of the improved function is still questioned. In the present study of dSP-B_{1-25}, we determine surface pressure-dependent changes in monolayer microstructure that are associated with the interactions of the dimeric peptide with lung surfactant lipids, and speculate about their role in the in vitro activities of this peptide.

The importance of SP-B studies in lung surfactants or in model systems appears from the lethal respiratory disease that is caused by SP-B insufficiency in humans.[18] A lack of effective surfactant, due to either immaturity in premature infants or various diseases in adults can result in respiratory distress syndrome (RDS).[15,16,22,23] Typical treatment uses exogenous replacement surfactants, but supplies of human lung surfactant are limited and therefore animal sources are most commonly used.[15,24−26] However, to minimize the risk of infection or immune responses, synthetic surfactants designed for specific RDS applications are a major goal of research.[6,7,11,27,28]

Although static surface tensions have been measured to be between 0 and 30 mN/m in excised lungs,[1,2] the dynamic surface tension during actual breathing is still unknown. Changes in alveolar surface area during respiration,[29] when compared to Langmuir isotherms of lung surfactants,[11] suggest that at least during extremes of the breathing cycle, the surface tension may range from 0 to 50 or more mN/m. Hence, understanding the surface properties of model lung surfactants over the entire range of surface pressures is likely to be necessary to the design of replacement lung surfactants. Langmuir monolayers at the air−water interface provide suitable model systems

(20) Beck, D. C.; Ikegami, M.; Na, C. L.; Zaltash, S.; Johansson, J.; Whtisett, J. A.; Weaver, T. E. *J. Biol. Chem.* **2000**, *275*, 3365−3370.
(21) Veldhuizen, E. J. A.; Waring, A. J.; Walther, F. J.; Batenburg, J. J.; Van Golde, L. M. G.; Haagsman, H. P. *Biohys. J.* **2000**, *79*, 377−384.
(22) Clements, J. A. *Arch. Environ. Health* **1961**, *2*, 280.
(23) Clements, J. A. *Physiologist* **1962**, *5*, 11−28.
(24) Shapiro, D. L.; Notter, R. H. *Surfactant Replacement Therapy*; Liss: New York, 1989.
(25) Robertson, B. *Clin. Physiol.* **1983**, *3*, 97−110.
(26) Robertson, B. In *International Symposium on Surfactant Replacement Therapy*; Lachmann, B., Ed.; Springer-Verlag: Rotterdam; Netherlands, 1987; pp 123−126.
(27) Phibbs, R. H.; Ballard, R. A.; Clements, J. A.; Heilbron, D. C.; Phibbs, C. S.; Schlueter, M. A.; Sniderman, S. H.; Tooley, W. H.; Wakely, A. *Pediatrics* **1991**, *88*, 1−9.
(28) Cochrane, C. G.; Revak, S. D. *Chest* **1994**, *105*, 57S-62S.
(29) Tschumperlin, D. J.; Margulies, S. S. *J. Appl. Physiol.* **1999**, *86*, 2026−2033.

for such studies because both, the molecular area and lateral pressure are directly accessible; thus, pressure−area measurements enable a straightforward physicochemical characterization. Care is necessary to extrapolate Langmuir monolayer behavior to lung surfactant behavior in vivo, but general correlations between in vitro and in vivo behavior are starting to emerge.[3,9,11,30,31]

In the present work we have employed pressure−area isotherms and Brewster-angle microscopy (BAM) measurements[32−35] to study the general phase behavior and morphology of lipid/SP-B mixtures in monolayers. Grazing incidence X-ray diffraction measurements[36,37] were applied in order to elucidate the influence of the lipid protein interaction on the ordering in the condensed lipid chain lattices on the angstrom scale. For the experiments, a full length SP-B_{1-78} and its amino terminus peptide dimer, dSP-B_{1-25}, were used. The measurements were performed with lipid mixtures that are believed to be able to serve as lipid replacements in RDS therapy.[6] This study provides new information on the lipid/SP-B protein interactions that could give an insight in the function of the protein and could help in engineering of lung surfactant replacements that are urgently needed in RDS therapy.[15,24,25,38]

Materials and Methods

Materials. Compounds 1,2-Dipalmitoyl-*sn*-glycero-3-phosphatidylcholine (DPPC) and 1-palmitoyl-2-oleyl-*sn*-glycero-3-phosphatidylglycerol (POPG) were purchased from Avanti Polar Lipids (Alabaster, AL; purity > 99%). Palmitic Acid (PA) was obtained from Sigma Chemical Co. (St. Louis, MO; purity > 99%). All lipid samples were used without further purification. The pure lipids were dissolved in chloroform/methanol (90/10 vol/vol).

Both, the native SP-B_{1-78} sequence and the N-terminal dimeric precursor peptide (see Figure 1) were synthesized on a 0.25 mmol scale with an ABI 431A peptide synthesizer using Fmoc chemistry as already described in the literature.[21,39] Solvents and ion pairing agents were removed from the peptide fractions followed by lyophilization from actonitrile/10 mM HCl (1/1 vol/vol). Dimeric dSP-B_{1-25} was prepared from the monomeric precursor using trifluorethanol: 10 mM phosphate buffer pH 7.5 (1/1 vol/vol) as described previously.[21] The expected molecular mass was confirmed by fast atom bombardment mass spectrometry, Electrospray and MALDI mass spectrometry (UCLA Center for Molecular and Medical Mass Spectrometry, Los Angels, CA).

Methods. The monolayer experiments have been performed using a home-built Langmuir trough equipped with a Wilhelmy-type pressuremeasuring device and two computer-controlled barriers that provided a symmetric compression. A lipid mixture **M1** of DPPC/POPG/PA (3/1/1 mol/mol) served as stock solution. The proteins were dissolved in $CHCl_3$/MeOH and added to the stock giving lipid protein mixtures with 10 wt % SP-B_{1-78} (**M2**) and dSP-B_{1-25} (**M3**), respectively. The mixtures were spread onto pure water (Millipore Milli-Q system, 18 MΩcm) or buffer (150 mM NaCl, 2 mM $CaCl_2$, 0.2 mM $NaHCO_3$, pH 7.0) subphases to form monolayers at the liquid−air interface.

For the BAM experiments, an argon ion laser was used as light source. A polarizer (Melles-Griot, Sunnyvale, CA) placed between laser and trough provided p-polarized light at the Brewster angle (approximately 53° from vertical for a pure water surface). The reflected light was collected using a simple lens (Melles-Griot) or a long focal microscopic objective (Nikon). An additional polarizer was used as analyzer in order to improve the contrast of the final images, which are detected by a Sony CCD camera (model XC-75). The images were recorded using a JVC super VHS VCR (Elmwood Park, NJ) and processed using a custom computerized data acquisition system.

Grazing incidence X-ray diffraction (GIXD) measurements[36,37,40] were performed on pure water as subphase at 20 °C using the liquid surface diffractometer on the beam line BW1 at HASYLAB, DESY, Hamburg, Germany. Experiments were performed at an angle of incidence of $0.85\alpha_c$ (α_c is the critical angle for total external reflection). A linear position sensitive detector (PSD) (OED-100-M, Braun, Garching, Germany) with a vertical acceptance $0 < Q_Z < 1.27$ Å^{-1} was used for recording the diffracted intensity as a function of both the vertical (Q_Z) and the horizontal (Q_{XY}) scattering vector components. The horizontal resolution of $Q_{XY} = 0.008$ Å^{-1} was determined by a Soller collimator mounted in front of the PSD.

Molecular Modeling. The dimeric dSP-B_{1-25} peptide was modeled using Insight/Discover 98.0 software (Molecular Simulations, San Diego, CA) on a Silicon Graphics Indigo-2R10000 High Impact workstation (Beckman Research Institute City of Hope Core Facility). The dimer was constructed using two SP-B_{1-25} monomers from the coordinates for the peptide in the Protein Data Bank (PDB: 1DFW). Cys-11 was mutated to alanine and the Cys-8 of one monomer was covalently linked to the Cys-8 of a second monomer to form a disulfide linkage. The torsional angles and bond lengths of the disulfide bonds were templated on those for a similar pair of connectivity's from the structure of NK-lysine (PDB: 1NKL) a protein that shares the same disulfide connectivity's and is in the same family (saposin proteins) as SP-B. The structure was then subjected to energy minimization and dynamics as described in [41] to determine a final covalently linked homodimer structure (see Figure 1).

Results

Figure 2 compares the first compression of the lipid mixture **M1** and the lipid protein systems (**M2**, **M3**) obtained for the monolayers on pure water (left, A) and on buffer (right, B). On pure water without protein (**M1**), the isotherm shows a "lift off" or first pressure increase at about 62 Å^2/molecule. On compression, linear regions of pressure increase dominate the isotherm. Between 20 and 30 mN/m, the slope increase indicates a drop in the compressibility of the film.

On addition of SP-B the 'lift-off' values are shifted toward larger molecular areas, resulting in 70 Å^2 for **M2** and 78 Å^2 for **M3,** respectively. The differences in the area values between **M1** and **M2**/**M3** decrease on increasing pressure. While **M2** shows only slight deviations, for **M3** much larger differences are found indicating a stronger interaction for dSP-B_{1-25}. Above 20 mN/m, the isotherm of **M2** is identical to that observed for **M1** while **M3** still exhibits significantly larger areas. At about 33 mN/m **M3** displays a pronounced plateau region and above 40 mN/m the isotherm corresponds to that observed for **M1**. All systems are stable up to high pressures above 60 mN/m. The collapse of the films occurs for **M1** and **M3** at 66 mN/m and **M2** at 69 mN/m.

(30) Johansson, J.; Curstedt, T. *Eur. J. Biochem.* **1997**, *244*, 675−689.
(31) Schürch, S.; Green, F. H. Y.; Bachofen, H. *Biochim. Biophys. Acta* **1998**, *1408*, 180−202.
(32) McConnell, H. *Annu Rev. Phys. Chem.* **1991**, *42*, 171−195.
(33) Möbius, D.; Möhwald, H. *Adv. Mater.* **1991**, *3*, 19−24.
(34) Hénon, S.; Meunier, J. *Rev. Sci. Instrum.* **1991**, *62*, 963−969.
(35) Lipp, M. M.; Lee, K. Y. C.; Zasadzinski, J. A.; Waring, A. J. *Rev. Sci. Instrum.* **1997**, *68*, 2574−2582.
(36) Als-Nielsen, J.; Jacquemain, D.; Kjaer, K.; Leveiller, F.; Lahav, M.; Leiserowitz, L. *Phys. Rep.* **1994**, *246*, 251−313.
(37) Kaganer, V. M.; Möhwald, H.; Dutta, P. *Rev. Mod. Phys. (USA)* **1999**, *71*, 779−819.
(38) Spragg, R. G.; Richman, P.; Gilliard, N.; Merritt, T. A. In *International Symposium on Surfactant Replacement Therapy*; Lachmann, B., Ed.; Springer-Verlag: Rotterdam; Netherlands, 1987; pp 203-211.
(39) Lipp, M. M.; Lee, K. Y. C.; Zasadzinski, J. A.; Waring, A. J. *Science* **1996**, *273*, 1196−1199.
(40) Jacquemain, D.; Leveiller, F.; Weinbach, S.; Lahav, M.; Leiserowitz, L.; Kjaer, K.; Als-Nielsen, J. *J. Am. Chem. Soc.* **1991**, *113*, 7684.
(41) Gordon, L. M.; Lee, K. Y. C.; Lipp, M. M.; Zasadzinski, J. A.; Walther, F. J.; Sherman, M. A.; Waring, A. J. *J. Peptide Res.* **2000**, *55*, 330−347.

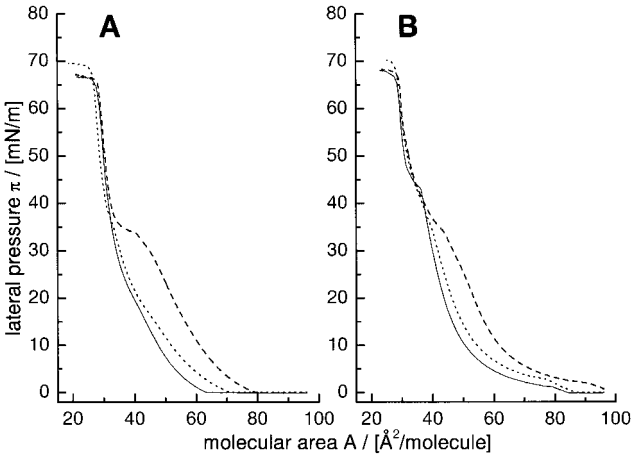

Figure 2. $\pi-A$ isotherms of the surfactant mixture **M1** (DPPC/POPG/PA = 3/1/1 mol/mol (—)) and lipid/surfactant protein SP-B mixtures **M2** (**M1** + SP-B_{1-78} (• •) and **M3** ((**M1** + dSP-B_{1-25} (- -) each containing 10 wt % SP-B. The molecular area was calculated in terms of area per average lipid molecule. The left plot (A) shows the isotherms taken on pure water; the right plot (B) displays the isotherms on saline buffer at 20 °C.

On buffer (right, B) the lift off values are shifted toward larger values for all systems investigated. **M1** exhibits a pronounced plateau region at low pressures indicating a first-order transition. At a higher pressure of 43 mN/m a small plateau region is observed, which could indicate a transition with a low enthalpy value. The two-phase coexistence region is also observed in the mixtures **M2** and **M3**, however at a slightly increased pressure. Additionally, **M2** exhibits only a kink in the pressure range of the small plateau of **M1** and **M3** shows a smeared out plateau at around 33 mN/m. Compared to SP-B_{1-78} (**M2**), dSP-B_{1-25} (**M3**) shows the larger effect on the areas in the low-pressure regions. However, the differences between **M1** and **M3** on buffer are smaller compared to the results obtained on pure water. In the high-pressure region above 50 mN/m, the isotherms are practically identical. Again, **M2** shows the highest collapse pressure (π_c = 70 mN/m) while the **M1** and **M3** exhibit the values already observed on pure water (66 mN/m).

Brewster angle microscopy (BAM) enabled the visualization of the morphology changes that occur during the compression of the monolayers. The contrast in BAM images is due to local differences in the monolayer refractive index caused by differences in local molecular density or packing. Figure 3A shows the results obtained with **M1**, **M2** and **M3** on water at 20 °C. At low lateral pressures, **M1** exhibits only small-condensed domains of a size below 10 μm. The behavior of sample **M1** at low pressures is similar to that of the clinical surfactant Survanta, which contains added palmitic acid.[11] Between 5 and 20 mN/m, the images show a homogeneous domain size distribution, before further increase in the surface pressure results in a decreased contrast. At a high pressure

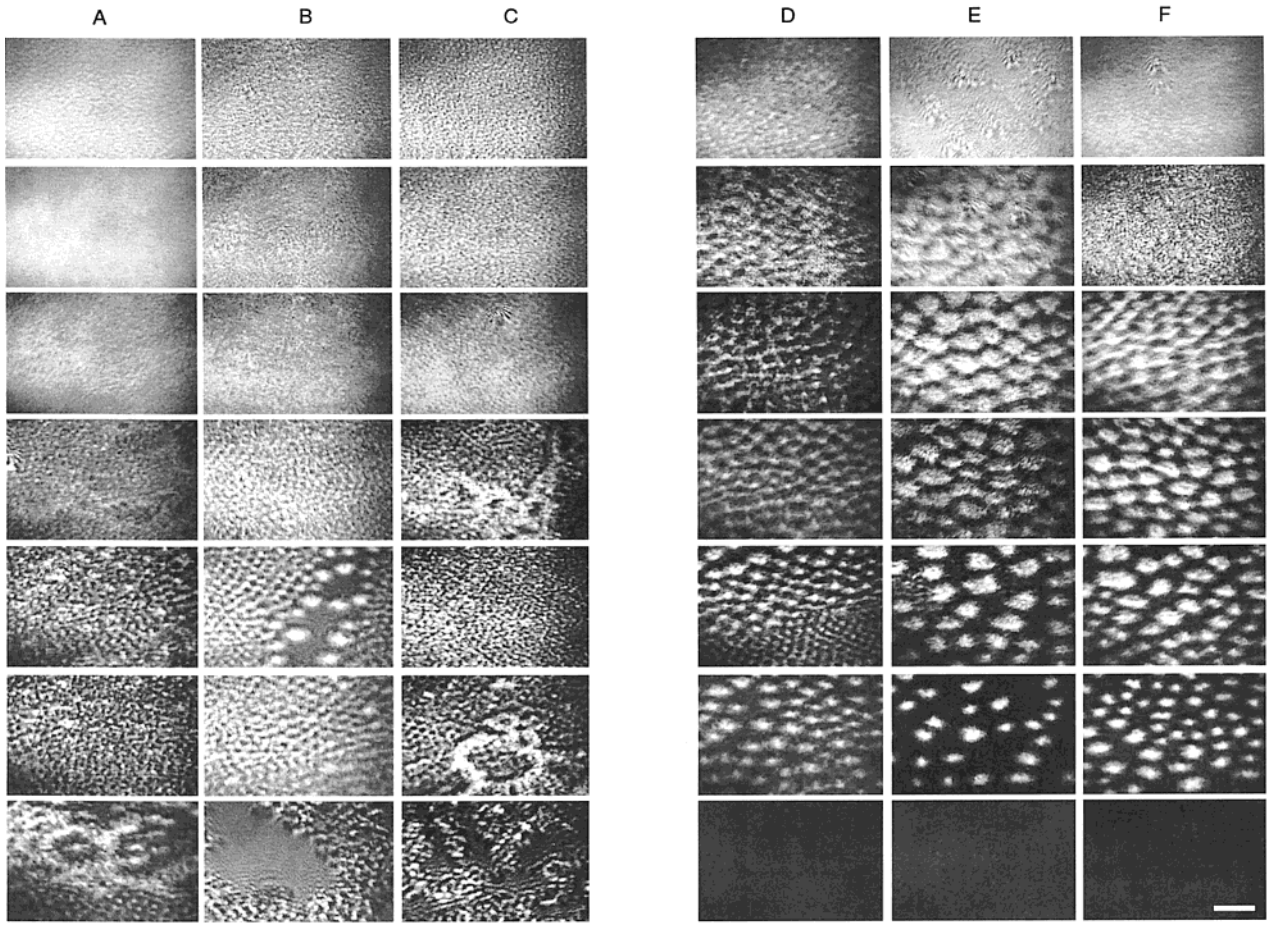

Figure 3. Brewster Angle micrographs of pure surfactant mixture **M1** (columns A and D) and of mixtures **M2** and **M3** with SP-B (columns B, C, E, F) on water (left) and buffer (right) at 20 °C. All mixtures contain a 3/1/1 (mol/mol) ratio of DPPC/POPG and PA. The weight percentage of SP-B_{1-78} (**M2**) and dSP-B_{1-25} (**M3**) was 10%. From bottom to top, each row corresponds to a certain lateral pressure (0, 5, 10, 20, 30, 40, and 60 mN/m). Contrast in the micrographs arises from coexistence of fluid (dark areas) and condensed domains (bright areas). By rotating analyzer in Brewster angle microscope, the bright domains can change to dark domains, which indicates the monolayer is tilted.

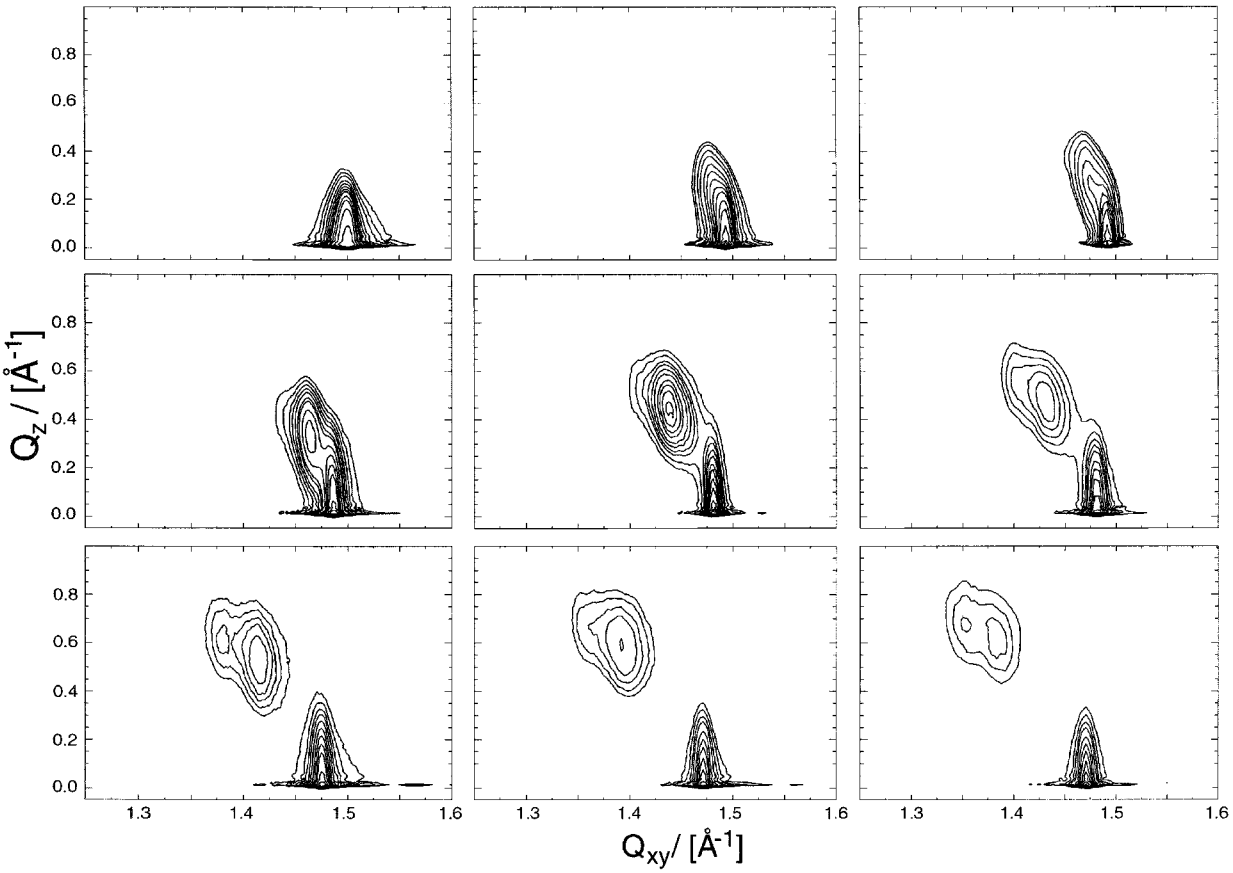

Figure 4. Contour plots of the corrected X-ray intensities versus in-plane scattering vector component Q_{XY} and out-of-plane scattering vector component Q_Z for surfactant mixtures **M1** (left), **M2** (middle), and **M3** (right) at different lateral pressures π (10, 25, and 40 mN/m, from bottom to top).

of 60 mN/m, the contrast increases again and small domains start to appear.

At zero pressure, both **M2** (SP-B_{1-78}, Figure 3B) and **M3** (dSP-B_{1-25}, Figure 3C) show small domains as found for **M1**, but in addition, gray regions of low contrast are observed that correspond to larger areas occupied by a liquid expanded phase. Increasing pressure leads to a more homogeneous morphology; however, for **M2** at 10 mN/m larger circular condensed domains with a size up to 50 μm are observed. As observed for **M1**, the transition toward a lack of contrast occurs at about 30 mN/m. At higher pressures of 40 mN/m, for both **M2** and **M3** the increase in contrast indicates a distribution of small domains while at this pressure **M1** shows low contrast images. Nevertheless, the resolution of the BAM is not sufficient to resolve the shape of the domains or their exact size.

On buffer at low pressures close to 0 mN/m, the images appear dark gray with no contrast, indicating a uniform liquid−expanded phase (see Figure 3D−F, bottom). These findings are in agreement with the isotherm measurements showing a fluidization of the monolayer on buffer. At 5 mN/m, bright circular condensed-phase domains with an average size of 40 μm in a continuous background of darker liquid−expanded phase occur. The images obtained for **M2** (Figure 3E) and **M3** (Figure 3F) appear darker, thus larger fractions of less ordered fluid structures have to be taken into account. Here, pressure increase between 10 and 20 mN/m is accompanied by an increasing domain size leading to diameters of about 70−80 μm at 20 mN/m. With increasing pressure, the large domains are replaced with much smaller structures. At a high pressure of about 60 mN/m, the lack of contrast that suggests the uniform orientation is observed for all samples investigated. The BAM images are consistent with the isotherms and show that both SP-B_{1-25} dimer and SP-B_{1-78} interact with the lipid monolayer and stabilize an expanded phase.

To get a better insight in possible structural changes of the condensed lipid-chain lattice induced by SP-B, GIXD was used to determine the in-plane structures in the condensed phase of the monolayers on the angstrom scale. GIXD is sensitive only to the ordered phases of the monolayer; the fluid phases only contribute to the background scattering. Figure 4 shows selected contour plots of the corrected X-ray diffraction intensities as a function of the in-plane scattering vector component Q_{XY} and the out-of-plane scattering vector component Q_Z for the mixtures **M1**, **M2**, and **M3** respectively.

Starting at low pressures, the system **M1** exhibits three low order diffraction peaks up to 25 mN/m (Figure 4, bottom left). Such an intensity profile is characteristic for an oblique chain lattice without mirror symmetry.[37] The maxima of the Bragg-rods are located above the horizon, thus the chains are tilted from the perpendicular orientation to the surface. The peak fit allows the calculation of lattice parameters, tilt angles, and area values given in Table 1. At 10 mN/m, the tilt amounts to (26 ± 1)° and the tilt azimuth is in a nonsymmetry direction. The fitted Bragg peak positions lead to spacings d ($d = 2\pi/Q_{XY}^{max}$) of 4.26, 4.44, and 4.56 Å, respectively. Increasing lateral pressure results in a shift to smaller lattice spacings and decreases the chain tilt. At 40 mN/m, the in-plane components Q_{XY} coincide, indicating hexagonal symmetry; however, intensity is observed up to high Q_Z values suggesting NN (nearest neighbor[37]) tilted chains with a small tilt of about (7 ± 1)°. At 50 mN/m, a single reflection

Table 1. Lattice Parameters (*A, B, γ*), Chain Tilt (*t*), Area Per Chain Perpendicular to Their Long Axis (A_0), and the Projected Area Per Chain (A_{xy}) in the Water Surface[a]

system	π	a (Å)	b (Å)	γ (deg)	t (deg)	A_{xy} (Å^2)	A_0 (Å^2)
M1	10	4.954	5.083	123.1	26 ± 1	22.6	20.2
	25	4.880	4.972	118.3	19 ± 1	21.4	20.4
	40	4.840	4.840	120.0	7 ± 1	20.3	20.1
	50	4.817	4.817	120.0	0	20.1	20.1
M2	10	4.990	5.126	115.3	29 ± 1	23.1	20.2
	25	4.914	5.029	117.2	22 ± 1	22.0	20.3
	40	4.908	4.871	120.2	10 ± 1	20.6	20.3
M3	10	5.005	5.134	114.9	30 ± 1	23.3	20.2
	17.5	4.960	5.079	116.0	27 ± 1	22.6	20.2
	25	4.926	5.031	116.9	23 ± 1	22.1	20.2
	35	4.880	4.979	118.0	18 ± 1	21.4	20.3
	40	4.859	4.943	118.6	15 ± 1	21.1	20.3

[a] The values are calculated from peak positions of the in-plane scattering vector component Q_{XY} and the out-of-plane component Q_Z of the diffraction signal that are obtained from peak fits using a Lorentzian model for Q_{XY} and a Gaussian model for Q_Z.

with a Bragg rod maximum at $Q_z^{max} = 0$ Å^{-1} indicates a hexagonal phase of upright oriented chains with spacings of 4.17 Å. Fitting the Bragg peak yields a full width at half-maximum of about 0.019 Å^{-1} that results in a correlation length of about 125 Å. Both the decrease in spacings and the chain tilt cause a decrease in the projected area per chain in the plane of the monolayer, A_{XY}, from 22.6 Å^2 (10 mN/m) to 20.1 Å^2 (50 mN/m).

Adding SP-B_{1-78} and dSP-B_{1-25} in **M2** and **M3** does not dramatically change the diffraction pattern found for **M1** at low lateral pressures (see Figure 4, bottom), but the fitted Bragg-peak maxima are slightly shifted toward lower values pointing to larger spacings at 10 mN/m (**M2**: 4.27 Å, 4.51 Å, 4.63 Å. **M3**: 4.27 Å, 4.54 Å, 4.66 Å). More pronounced differences in the GIXD intensity distribution of the samples are observed with increasing pressure where multiple reflections can be resolved up to 40 mN/m. Therefore, the chains are tilted and angles of (10 ± 1)° (**M2**) and (15 ± 1)° (**M3**) can be calculated.

Discussion

In this study, we have examined the influence of SP-B on the morphology (μm-scale) and the structure (angstrom scale) of monolayers formed by a lipid mixture that serves as good model for lung surfactants. SP-B fulfils a number of essential functions in lung surfactant monolayers, including promotion of lipid adsorption to the air−water interface, transport, and regulation of mechanical properties such as respreading of monolayers from post collapsed multilamellar structures. More recently was shown that SP-B also exhibits significant antimicrobial activity in vitro.[42,43]

The isotherm and BAM measurements for the pure ternary lipid mixture **M1** show that the monolayer on buffer is more expanded compared to water. Additionally only the isotherm on buffer exhibits first-order transitions. The first plateau at low pressure corresponds to a transition from a homogeneous liquid expanded to a condensed phase, which is supported by the BAM experiments (see Figure 3D−F, bottom). Above this transition the monolayer is always inhomogeneous, indicating a phase separation occurring together with the transition to the condensed state. However, from BAM images a phase separation between fluid phases cannot be excluded at low pressure. GIXD measurements show that the condensed part of the monolayer forms a homogeneous structure indicating no phase separation between condensed phases.

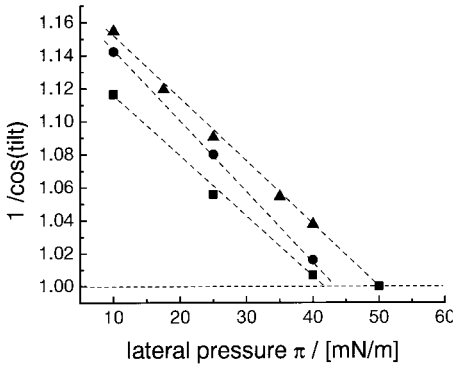

Figure 5. 1/cos(t) as function of the lateral pressure π for mixtures **M1** (■), **M2** (●), and **M3** (▲) with t as chain tilt angle to normal. The transition toward an upright oriented chain lattice is given by the linear extrapolation toward 1/cos(t) = 1.

SP-B alters the phase behavior of the Langmuir isotherms as well as the ordering in the two-dimensional model systems on different lengths scales by fluidization of the condensed lipid domains. Our isotherm measurements show that the addition of SP-B_{1-78} increases the molecular area significantly. At low pressures, the addition of dSP-B_{1-25} induces much larger changes, suggesting a more pronounced interaction of the lipid layer with the dimer. In previous studies, a formation of a fluid network that separates condensed phase domains and persists up to high lateral pressure was found.[39,44] A change of the collapse mechanism from heterogeneous nucleation/growth and fracturing processes toward a more homogeneous transition induced by a specific fatty acid−protein interaction was proposed. The lipid mixture used in our study does only contain a lower fraction of PA (20 mol %), but the BAM images taken at high pressure also show a high nucleation density and limited growth of the collapsed phase domains, indicating a comparable alteration of the more complex lipid mixtures **M2** and **M3**. The addition of SP-B changes the liquid expanded network observed for **M1** leading to larger area fractions occupied by the liquid expanded phase. On saline buffer, which mimics more physiological conditions, a pronounced stabilization of the network is obtained. Therefore, these findings might apply also under in vivo conditions.

Using GIXD our study demonstrates that changes in the structures of the condensed lipid domains must be considered. Using the area values calculated from the GIXD measurements allows the construction of an isotherm that accounts only for the well-ordered fraction of the monolayer. Assuming that A_{XY} is linear dependent on π and that A_0 is constant at 20 °C, 1/cos(t) = A_{XY}/A_0 should be linearly dependent on the lateral pressure π as shown in Figure 5. The transition pressure (π_C) toward the upright oriented hexagonal phase can then be estimated by extrapolation toward zero tilt. For the lipid mixture without protein (**M1**), this extrapolation results in a π_C-value of 41 mN/m. On addition of SP-B to the system, this transition is shifted toward higher pressures resulting in 44 mN/m for **M2** and 50 mN/m for **M3**, respectively.

Concurrently with the change in the tilt angle the projected area per chain, A_{XY}, is increased (see Table 1). A_{XY} decreases almost linearly with increasing pressure. At highest pressure, **M1** displays values of about 20.2

(42) Kaser, M. R.; Skouteris, G. C. *Peptides* **1997**, *18*, 1441−1444.
(43) Baatz, J. E.; Zou, Y.; Flume, P. A. *Am. J. Respir. Crit. Care Med.* **1999**, *159*, A895.
(44) Lipp, M. M.; Lee, K. Y. C.; Waring, A.; Zasadzinski, J. A. *Biophys. J.* **1997**, *72*, 2783−2804.

Å²/chain, which is typically reported for cross-sectional areas of double-chain lipids at 20 °C. The lipid−protein interaction obviously results in larger A_{XY} values in the whole pressure region indicating a less dense in-plane packing of the chains in the monolayer.

Comparing the A_{XY} values for **M1** and **M3** with the molecular area, A, from the pressure−area isotherms (Figure 1) yields smaller A_{XY} values in the low-pressure regions. This can be explained by the coexistence of condensed and fluid parts in the monolayers as seen by BAM. In the GIXD experiments only the condensed part of the monolayer contributes to A_{XY}, whereas lattice defects and fluid parts of the monolayer increase the molecular area, A, measured in the isotherms. Comparing the area values obtained from GIXD experiments with the molecular area it is obvious that in the low-pressure regions, the A_{XY}-values are smaller than the molecular areas. This can be explained by the coexistence of condensed and fluid parts in the monolayers as seen by BAM. In the GIXD experiments only the condensed part of the monolayer contributes to A_{XY}, whereas lattice defects and fluid parts of the monolayer increase the molecular area, A, measured in the isotherms. Comparing **M1** and **M3**, the latter shows larger deviations between A_{XY} and A indicating a protein supported increase of the fluid phase for **M3**. These findings can be explained assuming an adsorption of one helix of dSP-B_{1-25} at the domain boundary due to an electrostatic interaction with the hydrophilic headgroups leading to the observed changes in the lipid chain lattice. The second helix penetrates into the fluid part of the monolayer leading to the observed larger molecular areas. In contrast, the truncated monomeric peptide SP-B_{1-25} does not change the packing of simple fatty acid monolayers.[45] Here it was shown that the peptide is associated with the fatty acid monolayer, and that a portion of it is inserting into the monolayer. Based on the dimensions of the peptide derived from molecular simulations, an angle of insertion of the peptide of 56° normal to the interface was determined.[45]

Above 20 mN/m, the pure lipid mixture **M1** shows larger A_{XY} values compared to the isotherm measurement. In the BAM however, images without cracks or layer folds are observed in this medium-pressure region. Therefore, a loss of material mainly from the liquid-expanded phase into the subphase starting at about 20 mN/m must be assumed. In the case of **M3**, a plateau region at around 35 mN/m is observed. This indicates that dSP-B_{1-25} prevents the continuous loss of material observed at medium pressures for **M1**. GIXD measurements have shown that both SP-B_{1-78} and dSP-B_{1-25} induce larger tilt angles of the chains resulting from changes in the lipid headgroup region due to the adsorption of the proteins. Only in the case of dSP-B_{1-25} a penetration into the monolayer was found in the isotherm measurements, while SP-B_{1-78} does not insert into the lipid hydrophobic core. Therefore, we assume that above 35 mN/m the penetrated helix of dSP-B_{1-25} is squeezed-out from the monolayer and takes a defined fraction of mainly the fluid phase into the subphase forming a folded reservoir. The adsorbed helix remains at the interface and serves as an anchor that enables the reincorporation of the folded structures. Therefore, the peptide dimer leads to an increased reversibility upon compression−expansion cycles as also seen in isotherm measurements. On the other hand this model could support the findings from recent animal studies[20] showing enhanced activity of the peptide dimer compared to the monomer.

It must be assumed that the lipid composition of the fluid protein-rich phase differs from that of the condensed domains. The latter should mainly contain the condensed phase lipids PA and DPPC while the fluid phase most likely consists of the negatively charged POPG. Binding of the peptide should be predominantly driven by electrostatic interactions between the positively charged SP-B and the negatively charged PG or PA headgroups. Therefore, a specific lipid composition of the membrane is required for the proper function of SP-B in the native system.

We have shown that the addition of SP-B proteins to lipid mixtures of DPPC/POPG/PA has a drastic effect on surface properties, morphology and structures of the lipid films. The study indicates that SP-B can induce a modified collapse mechanism and regulates the re-spreading of the collapsed structures by formation of a fluid protein-rich network that is stabilized upon collapse. We presume that the main function of SP-B is the stabilization of a lipid reservoir close to the interface. The truncated dSP-B_{1-25} peptide is most effective in fulfilling this function, what could help to explain the higher activity found in vivo.

Abbreviations

BAM, Brewster angle microscopy
DPPC, rac. 1,2-dipalmitoyl-sn-glycerophosphocholine
GIXD, grazing incidence X-ray diffraction
PA, palmitic acid
RDS, respiratory distress syndrome
POPG, rac.-1-oleyl-2-palmitoyl-sn-glycerophosphocholine
SP-B, surfactant protein B, dSP-B_{1-25} dimer of the N-terminal sequence of SP-B

Acknowledgment. We gratefully acknowledge beamtime at the HASYLAB at DESY (Hamburg, Germany). We thank Dr. Mark Sherman of The City of Hope Molecular Modeling Core Facility (Cancer Center Support) for modeling of the dSP-B_{1-25} peptide. F.B. is grateful for financial support from the Deutsche Forschungsgemeinschaft (Emmy-Noether-Program Grant: BR 1826/2-1). J.A.Z., A.J.W., and J.D. acknowledge financial support from NIH Grant HL-51177, the University of California Tobacco Related Disease Research Program, Grant 8RT-0077, and Dissertation Award 8DT-0171.

LA015702W

(45) Lee, K. Y. C.; Majewski, J.; Kuhl, T. L.; Howes, P. B.; Kjaer, K.; Lipp, M. M.; Waring, A. J.; Zasadsinksi, J. A.; Smith, G. S. *Biophys. J.* **2001**, *81*, 572−585.